



**HAL**  
open science

# Exciting Vorticity Through Higher Order Bessel Beams With a Radial-Line Slot-Array Antenna

Davide Comite, Guido Valerio, Matteo Albani, Alessandro Galli,  
Massimiliano Casaletti, Mauro Ettore

► **To cite this version:**

Davide Comite, Guido Valerio, Matteo Albani, Alessandro Galli, Massimiliano Casaletti, et al.. Exciting Vorticity Through Higher Order Bessel Beams With a Radial-Line Slot-Array Antenna. IEEE Transactions on Antennas and Propagation, 2017, 65 (4), pp.2123 - 2128. 10.1109/TAP.2017.2670503 . hal-01551691

**HAL Id: hal-01551691**

**<https://hal.sorbonne-universite.fr/hal-01551691>**

Submitted on 12 Mar 2020

**HAL** is a multi-disciplinary open access archive for the deposit and dissemination of scientific research documents, whether they are published or not. The documents may come from teaching and research institutions in France or abroad, or from public or private research centers.

L'archive ouverte pluridisciplinaire **HAL**, est destinée au dépôt et à la diffusion de documents scientifiques de niveau recherche, publiés ou non, émanant des établissements d'enseignement et de recherche français ou étrangers, des laboratoires publics ou privés.

## Exciting Vorticity through Higher-order Bessel Beams with a Radial-Line Slot-Array Antenna

Davide Comite, Guido Valerio, Matteo Albani,  
Alessandro Galli, Massimiliano Casaletti, and Mauro Ettore

**Abstract**—In this paper, it is shown that a non-diffracting vortex beam (i.e., a higher-order Bessel beam with azimuthal phase variation) can be generated in the near field by synthesizing an inward cylindrical traveling-wave distribution over a finite aperture antenna. A radial line slot array (RLSA) is then designed to prove the concept. The collimated vortex beam is excited in the proximity of the RLSA, within a region properly defined by the non-diffracting range of the generated beam. The radial dependence of the longitudinal electric field of the vortex-beam magnitude follows a first-order Bessel function, and its phase presents a linear azimuthal variation. Full-wave results validate the generation of the non-diffractive higher-order Bessel beam within the radiative near-field of the launcher.

**Index Terms**—Near field, vortex beam, Bessel beam, radial line slot array (RLSA), orbital angular momentum (OAM).

### I. INTRODUCTION

Vortex beams are a class of electromagnetic waves carrying orbital angular momentum (OAM) thanks to a suitable angular phase variation on transverse planes [1], [2]. Due to their peculiar phase rotation, these beams have recently received a great interest at radiofrequencies and microwaves. Indeed, OAM can be potentially capable, among other applications, of an increased capacity of communication channels [3], enhanced remote sensing [4], and plasma control [5], [6].

Various antenna solutions have been proposed to radiate far fields carrying OAM (see, e.g., [1], [7]-[9] and references therein). On the other hand, fewer results are known about the focusing capabilities of vortex beams in the near field [10]-[12]. This result is in general hindered by diffraction phenomena, unless a specific class of non-diffracting beams is excited [13], [14]. The simplest kind of non-diffracting vortex beam can be derived through a higher-order Bessel beam. This beam presents transverse profile with Bessel-like radial dependence and a linear phase variation along the azimuthal angle. Higher-order Bessel beams are therefore an attractive solution to excite vorticity in a confined near-field region [11]. Besides, a polychromatic superposition of higher-order Bessel beams may allow the generation of non-diffracting twisted pulses carrying OAM [15].

A rigorously non-diffractive beam can only be excited by a transversely unbounded aperture. However, finite devices can generate such beam within a region in the near field of the radiating aperture known as non-diffractive range (NDR). At optical frequencies, higher-order Bessel beams have been synthesized by axicons [16], holographic surfaces [17], circular metallic slits [18], and quasi-periodic sheets [19]. These structures are illuminated by either plane waves or Laguerre-Gauss beams and may allow for the superposition of

different higher-order beams [20]. At microwaves, these solutions may result in cumbersome radiating systems due to the external source feeding the structure. Instead, the possibility to excite a focused beam by means of a pointwise source embedded in the antenna is very attractive. Previous works have mainly been focused on zeroth-order Bessel beams [21]-[24], i.e., azimuthally symmetric beams not carrying any OAM. The advantage of an embedded excitation is gained by means of simple leaky-wave launchers, using the interference between an outward and inward cylindrical traveling wave [22]. However, recent works have shown the possibility to generate non-diffractive Bessel beams by using only inward cylindrical traveling waves [25]. This solution avoids resonant radiating apertures for a wider band operation of the launcher. In this framework, the adoption of radial-line slot array (RLSA) antennas allow for the implementation of low cost, compact and highly efficient antenna centrally fed by a coaxial probe [24].

In this work, we prove the possibility to excite a non-diffractive higher-order Bessel beam with a traveling-wave illumination at microwaves. This result is subsequently used for the design of an RLSA antenna exciting a non-diffracting vortex beam with a linear azimuthal phase variation. This beam carries on an orbital angular momentum in the near field of the radiating structure. We focus here on an RLSA for its ease of fabrication and feeding system. To this aim, the near-field optimization procedure in [24] has suitably been modified and extended to take into account the phase profile of the considered aperture-field distribution. Besides, an in-house Method of Moments (MoM) [26] is used during the optimization process to carefully consider the mutual coupling amongst the slots and maximize the radiation efficiency. The optimization aims to synthesize both a given phase and amplitude distribution on the RLSA antenna aperture [27]. The final design has been validated by a commercial software. Field profiles for the longitudinal and transverse components of the radiated near field validate the design. The obtained results prove the possibility to excite a specific order in the near field of a RLSA. If the order of the OAM needs to be reconfigured, a more complex optimization procedure involving a multisource configuration should be applied. In this case, each source would excite a certain beam order. To this aim, recently, an RLSA design has been independently proposed and shown in [28], where a multi-source configuration selects the required beam order. However, the resulting design has been based on a standing-wave rather than an inward-wave illumination.

This paper is organized as follows. In Section II the exact aperture field distribution required to generate a non-diffractive beam with an azimuthal phase variation is introduced. The capabilities of an inward traveling-wave distribution to generate a non-diffractive higher-order beam are then discussed. Section III gives details on the design procedure exploited to synthesize the aperture field over an RLSA structure. Numerical results and full-wave simulations for the radiated near-field are shown in Section IV. Conclusion follows.

### II. DERIVATION OF THE APERTURE FIELD

In this section we compare the excitation of a higher-order Bessel beam through radial standing-wave and inward traveling-wave truncated apertures. In the following, a temporal dependence of the kind  $e^{j\omega t}$  is assumed and suppressed.

Let us consider an  $n$ th-order Bessel beam propagating along a  $z$  direction, being transverse-magnetic (TM) polarized with respect to  $z$ . In a cylindrical coordinate system  $(\rho, \phi, z)$ , the electric field components of the Bessel beam are

$$E_z(\rho, \phi, z) = E_0 J_n(k_{\rho a} \rho) e^{-jn\phi} e^{-jk_z z} \quad (1)$$

Manuscript received October 3rd, 2016, revised November 14th, 2016, accepted December 28th, 2016.

Davide Comite and Alessandro Galli are with the Department of Information Engineering, Electronics and Telecommunications, "Sapienza" University of Rome, 00184 Rome, Italy (comite@diet.uniroma1.it, galli@diet.uniroma1.it).

Guido Valerio and Massimiliano Casaletti are with Sorbonne Universités, UPMC Univ. Paris 06, F-75005 Paris, France (guido.valerio@upmc.fr, massimiliano.casaletti@upmc.fr).

Matteo Albani is with the Department of Information Engineering and Mathematics, University of Siena, 53100 Siena, Italy (matteo.albani@di.uisi.it).

Mauro Ettore is with Institut d'Electronique et de Télécommunications de Rennes (IETR) Université de Rennes 1, Avenue du Général Leclerc, 35042 Rennes, France (mauro.ettore@univ-rennes1.fr).

$$E_\rho(\rho, \phi, z) = -j \frac{k_{z_a}}{k_{\rho_a}} E_0 J'_n(k_{\rho_a} \rho) e^{-jn\phi} e^{-jk_{z_a} z} \quad (2)$$

$$E_\phi(\rho, \phi, z) = -\frac{nk_{z_a}}{k_{\rho_a}^2} E_0 \frac{J_n(k_{\rho_a} \rho)}{\rho} e^{-jn\phi} e^{-jk_{z_a} z} \quad (3)$$

where  $J_n(\cdot)$  is the  $n$ -order Bessel function of first kind,  $k_{\rho_a}$  the transverse propagation constant associated to the vortex beam, and  $k_{z_a} = \sqrt{k_0^2 - k_{\rho_a}^2}$  is the longitudinal (vertical) wavenumber,  $k_0$  being the free-space wavenumber. If  $n = 0$ , a zeroth-order azimuthally-symmetric beam is generated, whose normal component has a maximum along the  $z$ -axis. For  $n \neq 0$  an  $n$ th-order azimuthal phase variation is generated, whose normal component has a zero along the  $z$ -axis.

In order to generate the beam, one would need to excite a tangential electric field as (2)-(3) over an infinite aperture placed at  $z = 0$ :

$$E_\rho^{SW}(\rho, \phi, z = 0) = -j \frac{k_{z_a}}{k_{\rho_a}} E_0 J'_n(k_{\rho_a} \rho) e^{-jn\phi} \quad (4)$$

$$E_\phi^{SW}(\rho, \phi, z = 0) = -\frac{nk_{z_a}}{k_{\rho_a}^2} E_0 \frac{J_n(k_{\rho_a} \rho)}{\rho} e^{-jn\phi} \quad (5)$$

where the superscript SW stands for ‘‘standing-wave,’’ due to the presence of the radial standing-wave patterns  $J'_n$  and  $J_n$ .

As demonstrated in [22] with reference to zeroth-order beam, the truncation of this aperture with a finite radius  $\rho_a$ , required for physical realization, will limit the distance range where the beam is focused. A non-diffractive range can then be defined, from  $z = 0$  up to  $z_{\text{NDR}} = \rho_a \cot[\sin^{-1}(k_{\rho_a}/k_0)]$ . However, in order to provide a wider bandwidth of operation, one may prefer a radially traveling-wave excitation with respect to the radially standing-wave in (4), (5). To this aim, it was proved in [25] that an inward cylindrical wave  $H_0^{(1)'}$  (Hankel function of the first kind) can replace the standing-wave  $J_1$  in (2) to focus a zeroth-order Bessel beam in a suitable region of space.

Here, we adopt a similar approach to achieve a wide-band excitation of  $n$ th-order Bessel beams. To this aim, we numerically evaluate the fields excited by resonant and traveling-wave field distributions over a circular aperture of radius much larger than the relevant wavelength (and with respect to the finite size of a practical device) and over a finite circular aperture of radius  $\rho_a$ . The traveling-wave aperture field is obtained by replacing the  $J'_1$  and  $J_1$  functions with  $H_n^{(1)'}$  and  $H_1^{(1)}$ , respectively, in equations (4) and (5), yielding:

$$E_\rho^{IW}(\rho, \phi, z = 0) = -j \frac{k_{z_a}}{k_{\rho_a}} E_0 H_n^{(1)'}(k_{\rho_a} \rho) e^{-jn\phi} \quad (6)$$

$$E_\phi^{IW}(\rho, \phi, z = 0) = -\frac{nk_{z_a}}{k_{\rho_a}^2} E_0 \frac{H_n(k_{\rho_a} \rho)}{\rho} e^{-jn\phi} \quad (7)$$

where the superscript IW stands for ‘‘inward wave’’.

An outward traveling-wave field can also be considered, obtained by replacing the  $J'_n$  and  $J_n$  functions in equations (4), (5) with second-kind Hankel functions  $H_n^{(2)'}$  and  $H_n^{(2)}$ , respectively. Its expressions and the relevant results are omitted here for the sake of brevity (the diffracting behavior of this contribution for a zeroth-order implementation has been discussed in [25]).

We consider here as an example the generation of a vortex beam with  $n = 1$  and  $k_{\rho_a} = 0.4k_0$ , at the operating frequency  $f = 12.5$  GHz. However, the results can be easily reproduced at different frequencies and for different orders  $n$ . The field radiated in free space by each aperture distribution are evaluated numerically by means of Green’s function integrals by defining equivalent magnetic currents for the field profile over the aperture [29].

In Fig. 1, the magnitudes and phases of the  $z$ -component of the electric field excited by an infinite aperture (i.e., an aperture with

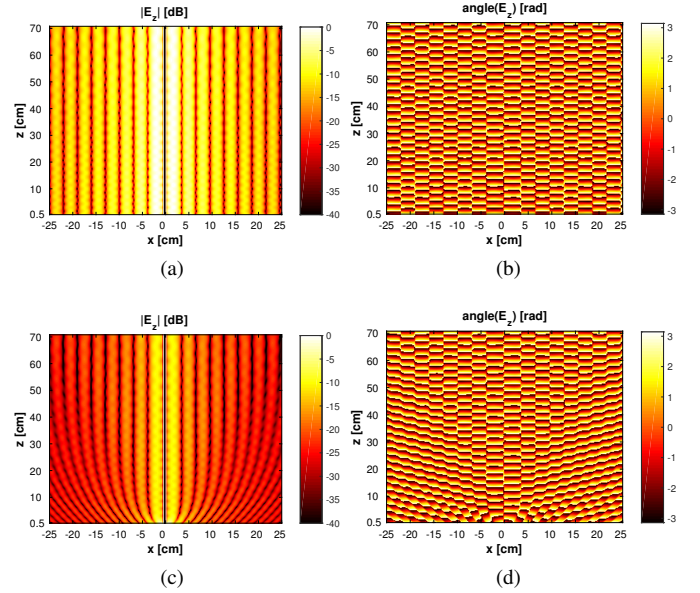


Fig. 1. Normalized normal component of the electric field ( $E_z$ ) radiated by an infinite ( $\rho_a \gg \lambda$ ) aperture. The field is plotted on a longitudinal plane ( $xz$ , i.e., orthogonal to the radiating aperture). Standing-wave distribution: (a) amplitude, (b) phase. Inward-wave distribution: (c) amplitude, (d) phase.

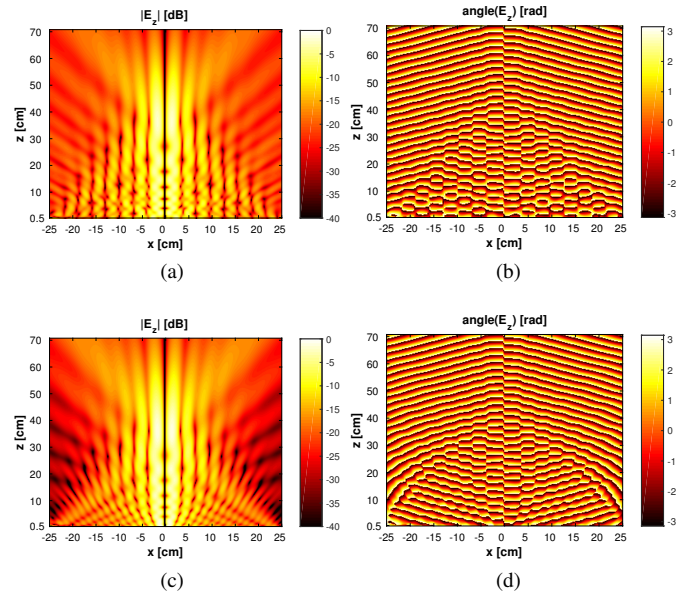


Fig. 2. As in Fig. 1 but for a finite circular aperture of radius  $\rho_a = 25$  cm.

radius  $\rho_a$  much larger than  $\lambda = 2.4$  cm) is presented. A standing-wave excitation is considered in Figs. 1(a) and (b), while an inward wave is considered in Figs. 1(c) and (d). As expected, the standing-wave excites a Bessel beam in the whole space. The inward wave excites the beam in a limited region of space, in agreement with the results highlighted in [25] concerning azimuthally-symmetric (i.e., zeroth-order) beams. In both cases it is possible to recognize the null of the magnitude on the  $z$  axis, the magnitude oscillations of the  $J_1$  functions, and a rotation of the phase typical of the vortex beam. In Fig. 2, the electric fields excited by a *finite* circular aperture with  $\rho_a = 25$  cm are shown. The same qualitative features of Fig. 1 can be remarked but, the finite aperture limits the non-diffractive range up to a distance  $z_{\text{NDR}} = 57.3$  cm along  $z$  in both cases. Figs.

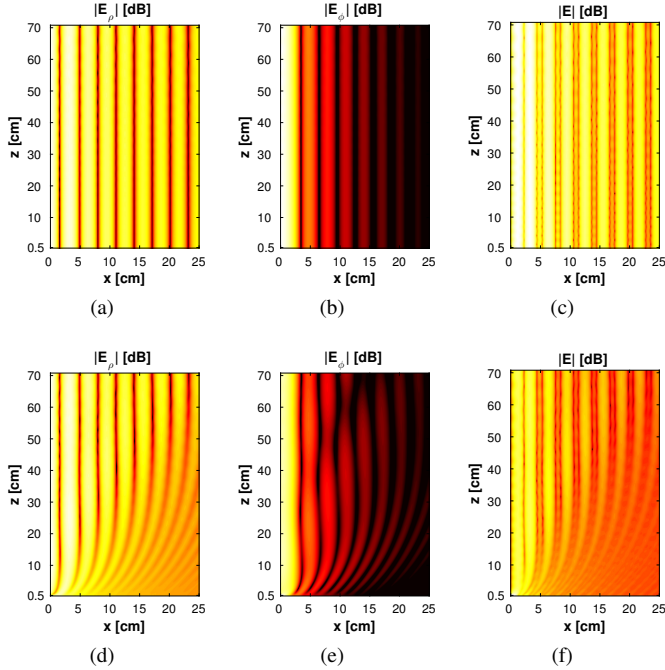


Fig. 3. Electric field excited by an infinite ( $\rho_a \gg \lambda$ ) aperture. (a)-(c) Magnitude of  $E_\rho$ ,  $E_\phi$ , and  $|E|$  excited by a standing-wave, (d)-(f) magnitude of  $E_\rho$ ,  $E_\phi$ , and  $|E|$  excited by an inward wave. Color scale as in Fig. 1.

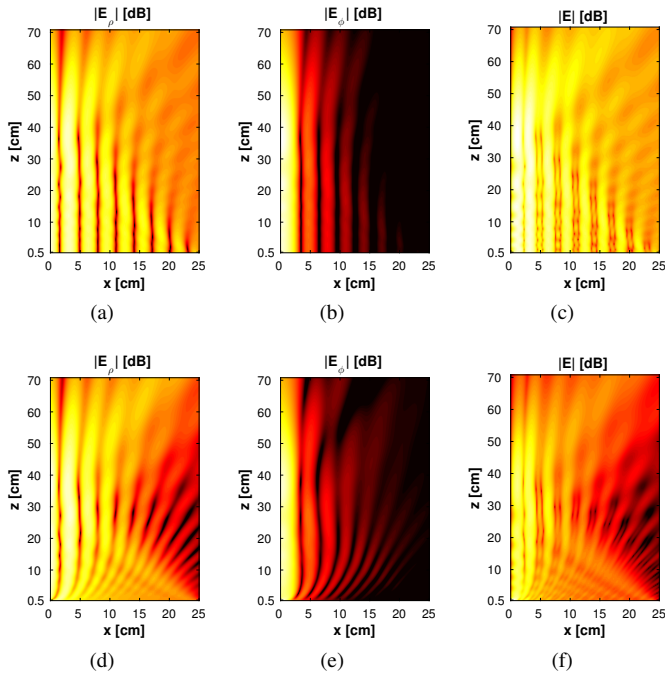


Fig. 4. Fields as in Fig. 3 but for a finite aperture ( $\rho_a = 25$  cm). (a)-(c) Magnitude of  $E_\rho$ ,  $E_\phi$ , and  $|E|$  excited by a standing wave, (d)-(f) magnitude of  $E_\rho$ ,  $E_\phi$ , and  $|E|$  excited by an inward-wave. Color scale as in Fig. 2.

3 and 4 present amplitude distributions of the radial and azimuthal components of the field from a infinite (i.e., having  $\rho_a \gg \lambda$ ) and finite aperture as well as the total field  $|E| = \sqrt{|E_\rho|^2 + |E_\phi|^2 + |E_z|^2}$ , respectively. As expected  $E_\rho$  shows a maximum along the vertical axis (where  $E_z$  presents a null). Furthermore,  $E_\phi$  shows a faster radial decay with respect to the other components, due to the extra  $\rho$  factor in the denominator of (3). These behaviors are in agreement with the

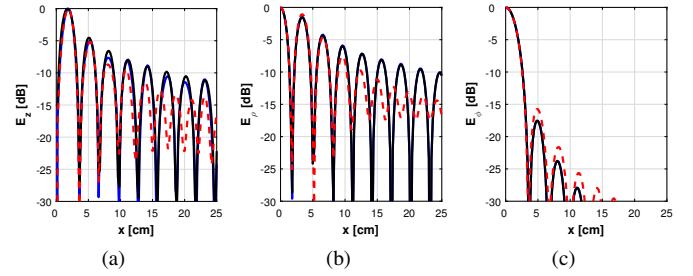


Fig. 5. Normalized electric-field components radiated by an infinite aperture ( $\rho_a \gg \lambda$ ) on the plane  $z = 10\lambda = 24$  cm by a standing-wave (blue line) and an inward wave distribution (red line). For comparison also the ideal field radiated by an infinite aperture (i.e., a Bessel profile represented by the function  $J_1(k_\rho \rho)e^{-j\phi}$ ) is reported (black line).

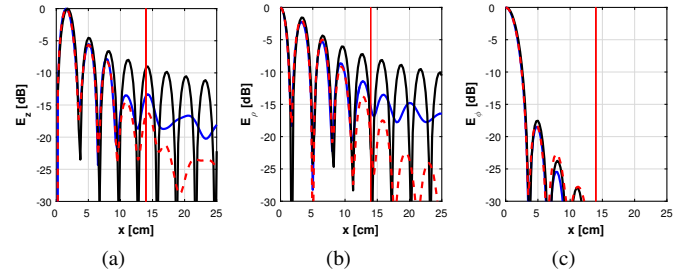


Fig. 6. Normalized electric-field components radiated by the finite aperture ( $\rho_a = 25$  cm) on the plane  $z = z_{\text{NDR}}/2 = 28.65$  cm by a standing-wave distribution (blue line) and an inward wave (red line). For comparison, the field radiated by an ideal infinite aperture (i.e., the Bessel profile  $J_1(k_\rho \rho)e^{-j\phi}$ ) is reported (black line). The vertical red line represents the region of validity of the inward approximation.

theoretical pattern described by (2) and (3). Specifically, as in the case discussed in [25], the field excited by an inward wave creates a non-diffractive vortex radiation close to the  $z$  axis, which can be regarded as a dominant geometrical-optics (GO) field contribution in a diffraction description of the radiating phenomenon.

To clearly evaluate the vortex-beam fields, Fig. 5 shows all the electric-field components excited by an infinite aperture at  $z = 10\lambda = 24$  cm. Both a standing and an inward wave are enforced (see the caption for the relevant details). As expected, the field radiated by the standing-wave is practically superimposed everywhere to ideal  $J_1$  functions. The field radiated by an inward wave agrees well with  $J_1$  functions close to the  $z$  axis, while the agreement is gradually deteriorated for larger radial distances. The fast radial decay of the  $\phi$  component is also clearly visible. In Fig. 6 the same comparison is reported for a finite aperture. The inward distribution is superimposed on both the ideal case (black curve) and the Bessel-like standing-wave case (blue curve) but is lost outside the region of validity of the GO contribution [25] (i.e., beyond the vertical red line).

Overall, these results clearly extend those in [25] to higher-order Bessel beams. In summary, arbitrary Bessel beams can be generated by traveling-wave aperture field distributions.

### III. SYNTHESIS OF THE APERTURE FIELD

In this section the field profile in (6) and (7) will be synthesized by means of an RLSA antenna. In order to simplify the design, only the  $\rho$  component (6) will be retained since the  $\phi$  component (7) is rapidly decaying with  $\rho$ . Final results will confirm the validity of this simplification.

We extend the optimization procedure proposed in [24] and [27] for RLSAs to take into account the phase variation of the aperture

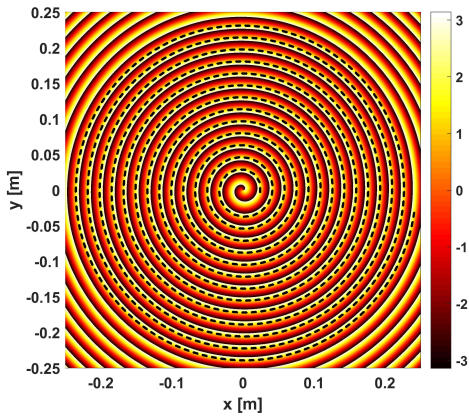


Fig. 7. Phase pattern obtained through interference. The slots follow a spiral arrangement according to (10).

field profile. The optimization procedure will provide the final slot layout for the RLSA. A slot etched into the metallic plane is modeled as an equivalent magnetic dipole proportional to the magnetic field  $\mathbf{H}^{inc}$  within the parallel-plate waveguide (PPW) through a dyadic polarizability  $\underline{\alpha}_m$  [27]. This property allows us to write

$$\mathbf{M} = \underline{\alpha}_m \cdot \mathbf{H}^{inc}. \quad (8)$$

For a single slot oriented along  $\mathbf{u}_0$ , the dyadic polarizability is given by  $\underline{\alpha}_m = \alpha_m \mathbf{u}_0 \mathbf{u}_0$ , where the amplitude of  $\alpha_m$  grows with the slot dimension up to the resonant length [27].

The aperture field distribution in (6) can be represented by the equivalent magnetic dipole moments of the RLSA slots, whose current distribution  $\mathbf{M}$  can be written as

$$\mathbf{M} = (\mathbf{E} \times \mathbf{z}_0)|_{z=0} = j \frac{k_{z_a}}{k_{\rho_a}} E_0 H_1^{(1)'}(k_{\rho_a} \rho) e^{-j\phi} \phi_0. \quad (9)$$

The current  $\mathbf{M}$  is then oriented along  $\phi_0$  and is a function of both  $\rho$  and  $\phi$ , due to the azimuthal dependence of the assumed TM modes. To synthesize the slot layout of the RLSA we apply a *holographic technique* to obtain the size and position of the slots of the array [27]. Initially the current distribution is approximated through the slots of the RLSA. The implementation of an ad-hoc optimization procedure is necessary to take into account the mutual coupling among slots, to minimize the error between theoretical and synthesized aperture field and to maximize the efficiency [24], [27]. For linear polarized RLSAs, whose slots are always orthogonal to the considered radius, this relation holds true:  $\underline{\alpha}_m = \alpha_m \mathbf{u}_0 \mathbf{u}_0 = \alpha_m \phi_0 \phi_0$ . The slot layout must result in a spiral arrangement described by

$$\rho = \frac{C}{k_{\rho_a} - k_d} \phi \quad (10)$$

$C$  being an arbitrary constant value and  $k_d$  the wavenumber of the field launched in the PPW. In the following, the sampling step  $\Delta s$  along the curve is arbitrary, and is considered a design parameter constrained between a minimum and a maximum value. It should be stressed that this procedure is different with respect to the one in [24], where no azimuthal variation of the phase is considered. Here the slots are arranged along a continuous curve and not anymore on concentric circumferences, making essential the control of  $\Delta s$  during the optimization process. To give a practical example, Fig. 7 presents the holographic pattern for the RLSA to synthesize an aperture field having an azimuthal phase variation of order  $n = 1$ . The spiral arrangement of the slots constituting the RLSA profile is clearly visible.

The theoretical and synthesized amplitude and phase of the magnetic dipole-moment distribution are compared in Fig. 8. A very good

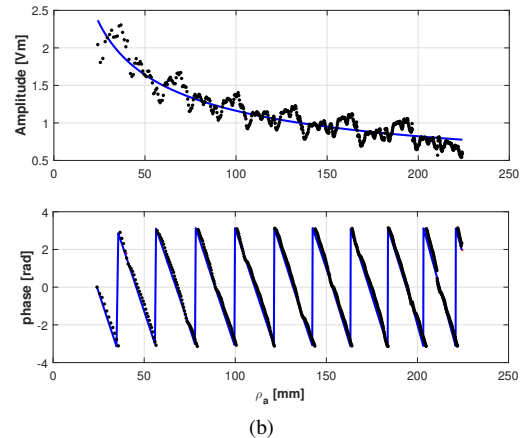
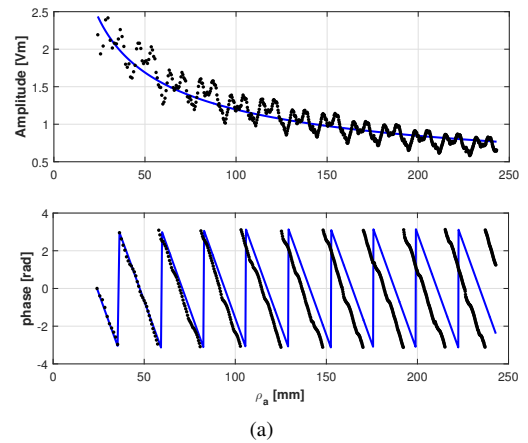


Fig. 8. Amplitude and phase distribution on the radiating aperture of the RLSA: the blue curves represent the target aperture field, black dots the synthesized aperture field. (a) amplitude (upper panel) and phase (lower panel) for the first step of the optimization procedure; (b) amplitude (upper panel) and phase (lower panel) for the last step of optimization.

agreement is obtained, confirming the accuracy and effectiveness of the proposed design. Fig. 8(a) shows the distribution at the first step of the procedure, whereas Fig. 8(b) shows the result after 231 iterations, when an excellent matching is obtained. This result is obtained by considering one basis function in the MoM code. It has been verified that increasing the number of functions up to 5 does not provide any appreciable improvement. A radiation efficiency  $\eta = 98\%$  has been obtained. It should be stressed that the RLSA has 779 slots. The design adopts a fast in-house MoM code [26], [24] and would not be compatible with usual commercial-software computation times.

#### IV. NUMERICAL RESULTS

In this Section we show the near field radiated by the RLSA designed in the previous section to validate the proposed design and concepts. The near fields have been computed by means of the in-house MoM [26] and have been compared with those of a full-wave commercial software, CST Microwave Studio [30]. The simulated structure is made by 779 slots whose length varies from 8 to 11.3 mm, the thickness of the PPW is  $h = 3.125$  mm with a finite radius  $\rho_a = 250$  mm. Fig. 9 shows the amplitude and phase of the normalized normal component of the electric field over a plane parallel to the radiating aperture at  $z = 32$  mm (about half the NDR) and for  $f = 12.5$  GHz. The amplitude of the field shows a good azimuthal invariance. The pattern of the first-order Bessel beam amplitude is clearly defined along with the correct null at the aperture

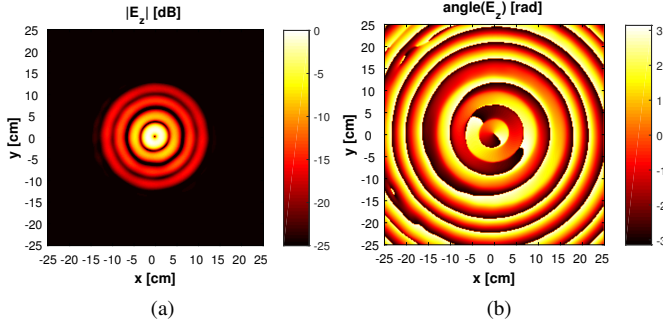


Fig. 9. Normalized  $E_z$  component for  $f = 12.5$  GHz by the in-house MoM for  $z = 32$  cm; (a) amplitude, (b) phase.

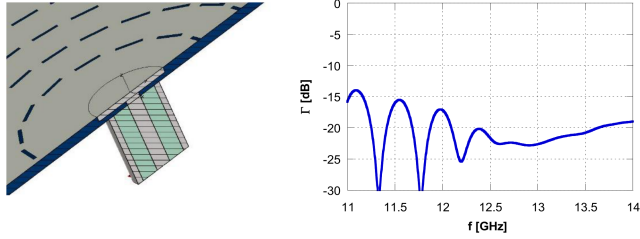


Fig. 10. Feeding system and reflection coefficient for the designed prototype.

center, coherently with (1). Furthermore, the azimuthal rotation of the phase on the transverse plane is very well defined.

The full-wave model is fed at the center using a coaxial probe transition, as shown in Fig. 10(a). The transition has been optimized for matching at the operating frequency. The return loss reported in Fig. 10(b) is below  $-10$  dB within a large band (11-14 GHz).

The 2-D amplitude and phase of the longitudinal  $E_z$  component on the  $xy$ -plane obtained through CST is shown in Fig 11(a)-(b) at the design frequency  $f = 12.5$  GHz. The observation plane is the same as in Fig. 9 (i.e.,  $z = 32$  cm). To avoid the full-wave simulation of a large domain, the aperture field (i.e., the equivalent source distribution) has been exported from the CST simulation, and the near-field has been evaluated on a fixed transverse or longitudinal plane by numerically solving the radiation integrals [29]. The results are in very good agreement with those obtained through the in-house MoM code shown in Fig. 9(a)-(b). In both cases the field amplitude shows a good azimuthal invariance, the pattern of the Bessel beam is well defined, and the azimuthal rotation of the phase is clearly visible. The accuracy of the proposed full-wave implementation is

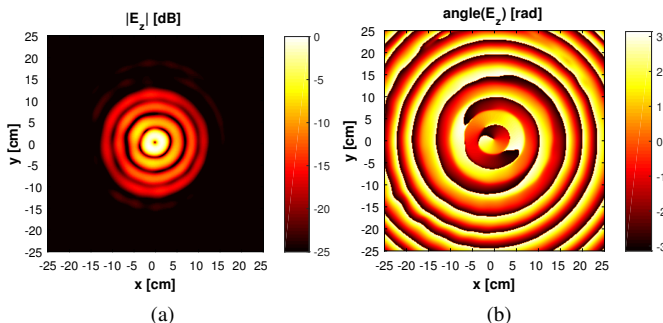


Fig. 11. Normalized  $E_z$  component for  $f = 12.5$  GHz by CST ( $z = 32$  cm, as in Fig. 9); (a) amplitude, (b) phase.

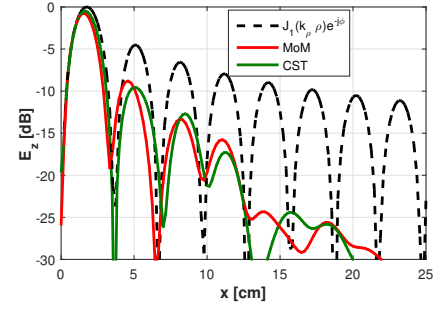


Fig. 12. Comparison of the 1-D field distribution along an arbitrary radius at  $z = 32$  cm for the ideal case (i.e., Bessel profile), the MoM field and the full-wave solution (CST).

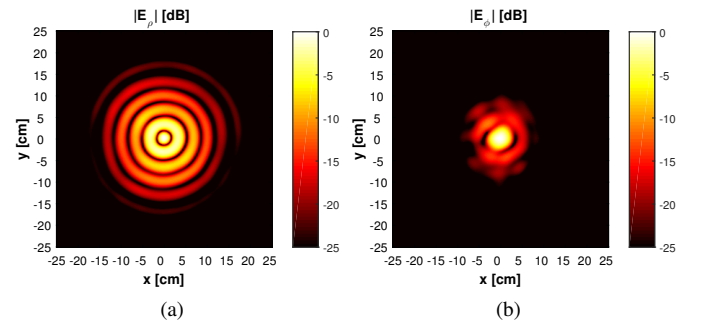


Fig. 13. As in Fig. 11: Normalized amplitude of (a)  $E_\rho$  and (b)  $E_\phi$ .

better appreciated in Fig. 12. This figure shows the normalized normal field component ( $E_z$ ) derived using the MoM code and CST along an arbitrary  $\phi$ -cut at  $z = 32$  cm. An excellent agreement is recognized between the ideal distribution (i.e., the field radiated by an ideal infinite aperture with a Bessel-like profile) and the MoM field. In Fig. 13(a) the amplitude of the radial component  $E_\rho$  of the field obtained with CST is presented. The field distribution is in agreement with the theoretical pattern provided by equation (2). These results further confirm the theoretical framework discussed in Section II. In Fig. 13(b), the amplitude of the azimuthal component is reported, whose behavior is in agreement with (3).

In Figs. 14(a)-(d) 2-D plots of the normalized electric field  $E_z$  are provided on the longitudinal plane (i.e.,  $xz$ -plane) at different frequencies. Once again, the null in the origin associated to the first-order Bessel function is well defined inside the non-diffracting region. As expected, the focusing effect is maximum at about half of the non-diffracting range  $z_{NDR}$ . The phase pattern along the  $z$ -direction is coherent with the relevant rotation on the  $xy$ -plane. Besides, the non-diffractive behavior is conserved within the considered band both in phase and in amplitude. The traveling-wave nature of the synthesized aperture distribution thus guarantees a wide-band operation. In addition, the frequency dispersion of the proposed structure produces a frequency-dependent non-diffracting range, that in turns is related to the variation of  $k_{\rho a}$ : larger values of the NDR are obtained as the frequency increases. However, as shown in Figs. 14(e) and (f) on the  $xy$  plane, the launcher still generates well-defined phase patterns for the Bessel beam with the expected azimuthal phase variation. Such large bandwidth behavior may pave the way for the generation of twisted X-waves (i.e., pulses), that have been recently studied at optical frequencies [15], [31], whose experimental validation is still lacking in the microwave and mm-wave ranges.

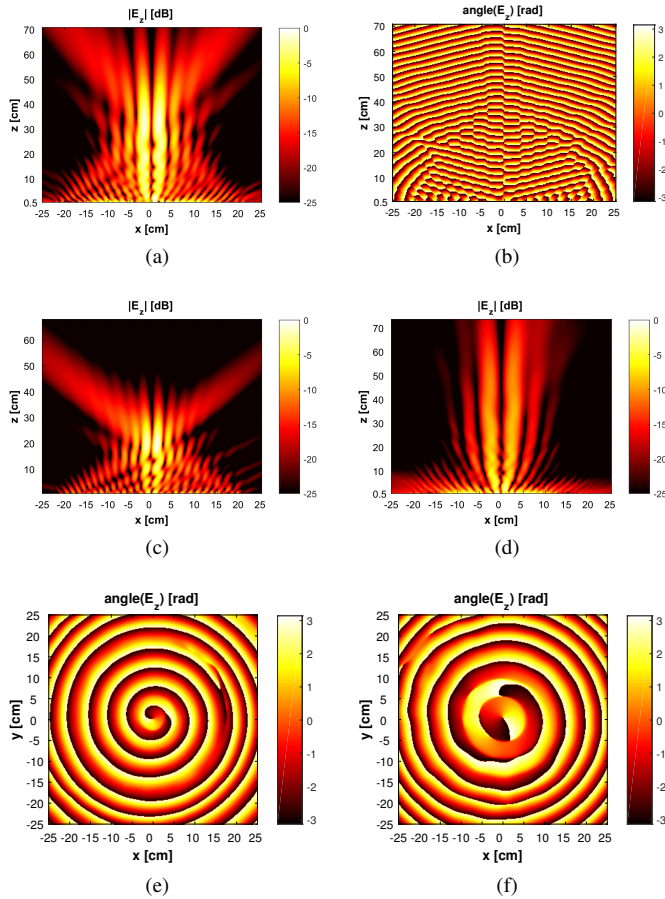


Fig. 14. Normalized  $E_z$  component on a longitudinal plane by CST; (a) amplitude and (b) phase at 12.5 GHz; (c) amplitude and (d) 13.5 GHz. Phase on the  $xy$  plane at (e) 11.5 GHz and (f) 13.5 GHz.

## V. CONCLUSION

The generation of a higher-order Bessel beam having an azimuthal phase variation using an inward cylindrical traveling-wave distribution has been discussed. An RLSA structure has been designed to synthesize such aperture-field profile and validate the concept at microwaves. Both the amplitude and the phase of the radiated field over the longitudinal and transverse planes have been computed, showing the radial and azimuth dependence over the non-diffractive range. The non-diffractive properties of different components of the excited electric field have also been discussed. The proposed solution is particularly interesting for areas such as near-field probing, and for the OAM applications. Thanks to the traveling-wave nature of the structure, potential wide-band applications could be envisaged in future works.

## REFERENCES

- [1] S. V. Mohammadi, L. K. Daldorff, J. E. Bergaman, R. L. Karlsson, B. Thidé, K. Forozesh, T. D. Carozzi, and B. Isham, "Orbital angular momentum in radio - A system study," *IEEE Trans. Antennas Propag.*, vol. 58, no. 2, pp. 565–572, Feb. 2010.
- [2] A. Al-Bassam, M. Salem, and C. Caloz, "Vortex beam generation using circular leaky-wave antenna," in *IEEE Antennas Propag. Soc. Int. Symp.*, July 2014, pp. 1792–1793.
- [3] E. Mari, F. Spinello, M. Oldoni, R. A. Ravanelli, F. Romanato, and G. Parisi, "Near-field experimental verification of separation of OAM channels," *IEEE Ant. Wireless Propag. Lett.*, vol. 14, pp. 566–558, 2015.
- [4] N. Urribe-Patarroyo, A. Fraine, D. S. Simon, O. Minaeva, and A. V. Sergienko, "Object identification using correlated orbital angular momentum states," *Quantum Physics*, 5 pp., Sep. 2012.

- [5] Y. Yasaka, K. Koga, N. Ishii, T. Yamamoto, M. Ando, and M. Takahashi, "Planar microwave discharges with active control of plasma uniformity," *Physics of Plasmas*, vol. 9, no., pp. 1029–1035, Mar. 2002.
- [6] T. Yamamoto, M. Ono, M. Ando, N. Goto, N. Ishii and Y. Yasaka, "Near-field distribution of radial line slot antenna for surface-wave-coupled plasma generation," *J. Appl. Phys.*, vol. 40, pp. 380–387, Jan. 2001.
- [7] R. Niemiec, C. Brousseau, K. Mahdjoubi, O. Emile, and A. Ménard, "Characterization of an OAM flat-plate antenna in the millimeter frequency band," *IEEE Ant. Wireless Propag. Lett.*, vol. 13, pp. 1011–1014, 2014.
- [8] N. J. G. Fonseca, L. Coulomb and J. Angevain, "A Fresnel-like reflector antenna design for high-order orbital angular momentum states," *European Conf. Antennas Propag. (EuCAP)*, 2015.
- [9] Z. Zhang, S. Xiao, Y. Li, and B. Wang, "A circularly polarized multimode patch antenna for the generation of multiple orbital angular momentum modes," *IEEE Antennas Propag. Lett.*, in press.
- [10] K. Huang, P. Shi, G. W. Cao, K. Li, X. B. Zhang, and Y. P. Li "Vector-vortex Bessel-Gauss beams and their tightly focusing properties," *Opt. Lett.*, vol. 36, no. 6, pp. 888–890, Mar. 2011.
- [11] C. J. Sheppard "Polarized focused vortex beams: half-order phase vortices," *J. Opt. Soc. Amer. A*, vol. 22, no. 15, pp. 18128–41, Jul. 2014.
- [12] C. Guclu, M. Veysi, and F. Capolino, "Vector vortex beam transmitarrays composed of split-ring slot element," *IEEE Antennas Propag. Soc. Int. Symp.*, Vancouver, BC, Canada, 2015.
- [13] M. Born and E. Wolf *Principles of Optics*. Pergamon Press, 1970.
- [14] J. Durnin, "Exact solutions for non-diffracting beams. I. The scalar theory," *J. Opt. Soc. Amer. A*, vol. 4, no. 4, pp. 651–654, Apr. 1987.
- [15] M. Ornigotti, C. Conti, and A. Szameit. "Effect of orbital angular momentum on non-diffracting ultrashort optical pulses," *Phys. Rev. Lett.*, vol. 115, 100401-5, 2015.
- [16] J. Arlt and K. Dholakia, "Generation of high-order Bessel beams by use of an axicon," *Opt. Commun.* vol. 177, pp. 297–301, 2000.
- [17] A. Vasara, J. Turunen, and A. T. Friberg, "Realization of general nondiffracting beams with computer-generated holograms," *J. Opt. Soc. Am. A*, vol. 6, no. 11, Nov. 1989.
- [18] H. S. Lee, B. W. Stewart, K. Choi, and H. Fenichel, "Holographic non-diverging hollow beam," *Phys. Review A*, vol. 49, no. 6, Jun. 1994.
- [19] L. Li and Y. Tan, "Theoretical analysis of vector-vortex fields generated by quasi-periodic planar structure," *IEEE Ant. Wireless Propag. Lett.*, vol. 13, pp. 487–490, 2014.
- [20] R. Vasilyeu, A. Dudley, N. Khilo, and A. Forbes, "Generating superpositions of higher-order Bessel beams," *Opt. Exp.*, vol. 17, no. 26, Dec. 2009.
- [21] S. Chavez-Cerda, "A new approach to Bessel beams," *J. Mod. Opt.*, vol. 46, pp. 923–930, 1999.
- [22] M. Ettorre and A. Grbic, "Generation of propagating Bessel beams using leaky-wave modes," *IEEE Trans. Antennas Propag.*, vol. 60, no. 8, pp. 3605–3613, Aug. 2012.
- [23] P. Lemaître-Auger, S. Abielmona, and C. Caloz, "Generation of Bessel beams by two-dimensional antenna arrays using sub-sampled distributions," *IEEE Trans. Antennas Propag.*, vol. 61, no. 4, pp. 1838–1849, Apr. 2013.
- [24] M. Ettorre, M. Casaletti, G. Valerio, R. Sauleau, L. Le Coq, S. C. Pavone, and M. Albani. "On the near-field shaping and focusing capability of a radial line slot array," *IEEE Trans. Antennas and Propag.*, vol. 62, no. 4, pp. 1991–1999, Apr. 2014.
- [25] M. Albani, S. C. Pavone, M. Casaletti, and M. Ettorre, "Generation of non-diffractive Bessel beams by inward cylindrical traveling wave aperture distributions," *Opt. Exp.*, vol. 22, no. 15, pp. 18354–18364, Jul. 2014.
- [26] M. Casaletti, G. Valerio, J. Seljan, M. Ettorre, and R. Sauleau, "A full-wave hybrid method for the analysis of multilayered SIW-based antennas," *IEEE Trans. Antennas Prop.*, vol. 61, no. 11, pp. 5575–5588, Nov. 2013.
- [27] M. Albani, A. Mazzinghi, and A. Freni, "Automatic design of CP-RLSA antennas," *IEEE Trans. Antennas Propag.*, vol. 60, no. 12, pp. 5538–5547, Dec. 2012.
- [28] A. Mazzinghi, A. Freni, "RLSA antenna for generating vortex modes in near-field radiating zone for radar applications," in *IEEE Antennas Propag. Soc. Int. Symp.*, Fajardo, Puerto Rico, USA, 2016.
- [29] R. F. Harrington, *Time-harmonic electromagnetic fields*. Wiley IEEE-press, 1961.
- [30] CST Products, available online: www.cst.com, Germany, v. 2015.
- [31] J. Salo, J. Fagerholm, A. T. Friberg, and M. M. Salomaa, "Unified description of nondiffracting X and Y waves," *Phys. Rev. Lett. E*, vol. 62, 4261, 2000.